Lecture notes on topological insulators

Ming-Che Chang

Department of Physics, National Taiwan Normal University, Taipei, Taiwan

(Dated: December 30, 2021)

Contents

I. WEYL SEMIMETAL

There are two important types of nodal points in 3D. One is the point degeneracy between two energy levels, the other is the point degeneracy between four energy levels, see Fig. 1. To distinguish between them, from now on we call the former a **Weyl point**, and the latter a **Dirac point**. In this and the following chapter, we will study the Weyl point.

A. Classification of Weyl node

The Hamiltonian near a Weyl point can be written as

$$\mathsf{H} = \mathbf{d}(\mathbf{k}) \cdot \boldsymbol{\sigma}, \tag{1.1}$$

where $\mathbf{k}$ is the momentum away from the node. If the components of $\mathbf{d}$ are all linear in $\mathbf{k}$, then we call it a **linear Weyl node**. If at least one of the components of $\mathbf{d}$ is quadratic in $\mathbf{k}$, then we call it a **quadratic Weyl node**, and so on.

The **topological charge** (or Berry index) of a node is

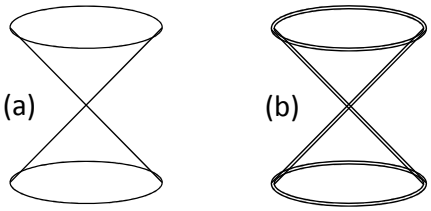

FIG. 1 (a) A Weyl point between two levels. (b) A Dirac point between 2 double-degenerate levels.

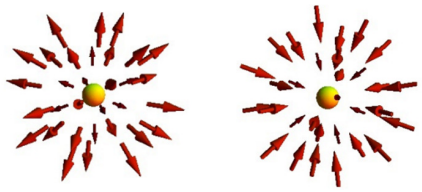

FIG. 2 The textures of $\mathbf{d}(\mathbf{k})$ of two Weyl points with opposite helicities. The figures are from somewhere on the web.

given by the first Chern number (see Sec. **??**),

$$Q_T = \frac{1}{2\pi}\int_{S^2_{\mathbf{k}}} d^2\mathbf{k}\cdot\mathbf{F}, \tag{1.2}$$

$$F_k = \frac{1}{2d^3}\mathbf{d}\cdot\frac{\partial\mathbf{d}}{\partial k_i}\times\frac{\partial\mathbf{d}}{\partial k_j}. \tag{1.3}$$

The integral is over a constant-energy surface with fixed $|\mathbf{d}|$, and i, j, k are in cyclic order. We learned in Sec **??** that the integrand is just (half of) the solid angle of the image $f : S^2_{\mathbf{k}} \to S^2_{\mathbf{d}}$, thus Q_T is the winding number of the map.

For example, consider

$$\mathsf{H} = \pm\mathbf{k}\cdot\boldsymbol{\sigma}, \tag{1.4}$$

the textures of $\mathbf{d}(\mathbf{k}) = \pm\mathbf{k}$ around the nodal point are shown in Fig. 2. It is obvious that the winding numbers, and hence the topological charges, are ±1. The sign $\pm$ is called the **helicity** (or **chirality**) of the Weyl point.

For a general linear node, its topological charge remains to be $+1$ or -1. Its sign can be determined by the sign of the Jacobian of the map $\mathbf{k}\to\mathbf{d}(\mathbf{k})$,

$$Q_T = \mathrm{sgn}\left|\frac{\partial d_i}{\partial k_j}\right|, \tag{1.5}$$

which is the same for every point $\mathbf{k}$. The sign simply shows that whether the map preserves or reverses the orientation.

For a Weyl node with higher order, its topological charge can also be determined by the energy dispersion near the node. This is explained below (see the App. of Chang and Yang, 2015) : An image point $\mathbf{d}^r$ is called a **regular point** if the Jacobian $|\partial d^r_i/\partial k_j| \neq 0$. A regular point can have none, or several pre-image points $\mathbf{k}^{(\ell)}$, $\mathbf{d}(\mathbf{k}^{(\ell)}) = \mathbf{d}^r, \ell = 1, \cdots, N$. The degree of the map f is defined as,

$$\deg f = \sum_{\ell=1}^{N} \mathrm{sgn}\left(\left|\frac{\partial d_i}{\partial k_j}\right|_{\mathbf{k}=\mathbf{k}^{(\ell)}}\right). \tag{1.6}$$

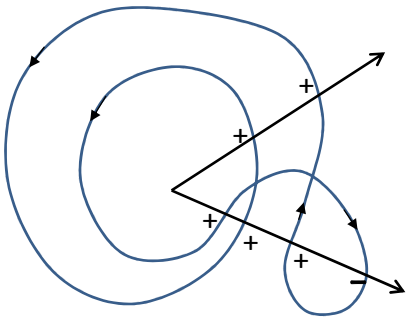

FIG. 3 The winding number is determined by the degree of the map, which is the same irrespective of the direction one peeps.

It is equal to the winding number, and thus the topological charge $Q_T = \deg f$. **Brouwer's lemma** guarantees that $\deg f$ is the same for every regular points. For an illustration of the winding number for a 1D loop around a point, see Fig. 3. Therefore, one can choose a convenient $\mathbf{d}^r$ to calculate it. For more details, see Sec. 10.7 of Felsager, 1998, or Milnor, 1965.

For example, for the following quadratic Weyl node,

$$\mathbf{d}(\mathbf{k}) \simeq \left(\frac{k_y^2}{2} - \frac{k_x^2}{2}, k_x k_y, \pm k_z \right), \tag{1.7}$$

the Jacobian is

$$\left| \frac{\partial d_i}{\partial k_j} \right| = \mp (k_x^2 + k_y^2). \tag{1.8}$$

Choose $\mathbf{d}_0 = (1/2, 0, 0)$, then there are two pre-images, $\mathbf{k}^{(1)} = (0, 1, 0)$ and $\mathbf{k}^{(2)} = (0, -1, 0)$. They contribute to $Q_T = \mp 2$ in total. A node with $|Q_T| = 2$ is called a **double Weyl node**.

If $d_x(\mathbf{k})$ is changed to $(k_x^2 + k_y^2)/2$, then the topological charge would be 0. That is, not all quadratic Weyl nodes are double Weyl nodes.

B. Linear Weyl node

In the following, we focus only on the linear Weyl node. Its gauge structure is similar to that of a magnetic monopole. For example, for the nodal point in Eq. (1.4), the Berry curvature is

$$\mathbf{F} = \mp \frac{1}{2} \frac{\hat{\mathbf{k}}}{k^2}, \tag{1.9}$$

which is the same as the magnetic field of a monopole. (Cf: Berry curvatures of various 2D systems in Sec. **??**.)

Once a Weyl node exists, it is stable against perturbations. Consider

$$H = \pm v \mathbf{k} \cdot \boldsymbol{\sigma} + H', \tag{1.10}$$

TABLE I Counting Weyl nodes

time-rev symm	space-inv symm	min number
×	×	2
○	×	4
×	○	2
○	○	unstable

H' is an arbitrary perturbation that can be expanded by Pauli matrices,

$$H' = a(\mathbf{k}) + \mathbf{b}(\mathbf{k}) \cdot \boldsymbol{\sigma} \tag{1.11}$$

$$= a(\mathbf{k}) + \mathbf{b}(0) \cdot \boldsymbol{\sigma} + \boldsymbol{\sigma} \cdot \sum_j \left. \frac{\partial \mathbf{b}}{\partial k_j} \right|_0 k_j + O(k^2). \tag{1.12}$$

It's obvious that the second term shifts the position of the node, the third renormalizes the velocity of the Weyl electron, but no gap is opened. That is, the Weyl point remains intact under an arbitrary perturbation. It could disappear *only by merging with another node with opposite topological charge.*

1. Multiplet of nodes due to symmetry

First, in *odd* spatial dimension, in the absence of space or time symmetry, massless lattice fermions are required to appear in pairs with opposite helicities. This is the **Nielsen-Ninomiya theorem** (Nielsen and Ninomiya, 1981a,b), or **fermion-doubling theorem** (see App. **??**). A simple explanation is as follows (Armitage *et al.*, 2018): If we surround a Weyl point at $\mathbf{k}_0$ with a closed surface S, the the Berry flux through S is $2\pi Q_T$. We can inflate this surface S to cover the whole BZ. But because of the periodicity of the BZ, $\partial BZ = 0$. Hence the total Berry flux should be zero. This implies that there must be another Weyl point with an opposite topological charge inside the BZ.

We now consider one node with helicity + or −,

$$\mathsf{H} = \pm v (\mathbf{k} - \mathbf{k}_0) \cdot \boldsymbol{\sigma}. \tag{1.13}$$

Under time-reversal transformation (if the pseudo-spin behaves like a spin),

$$\mathbf{k} \to -\mathbf{k}, \quad \boldsymbol{\sigma} \to -\boldsymbol{\sigma}. \tag{1.14}$$

So

$$\mathsf{H} \to \mathsf{H}' = \pm v (\mathbf{k} + \mathbf{k}_0) \cdot \boldsymbol{\sigma}. \tag{1.15}$$

Therefore, if there is TRS, then there must be another nodal point at $-\mathbf{k}_0$ with the same helicity.

Under space-inversion transformation,

$$\mathbf{k} \to -\mathbf{k}, \quad \boldsymbol{\sigma} \to \boldsymbol{\sigma}. \tag{1.16}$$

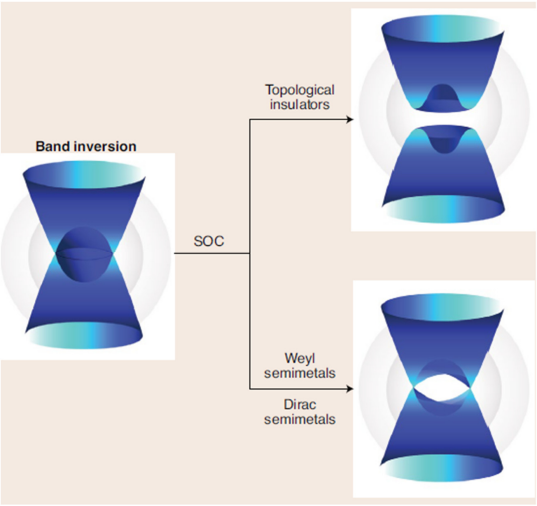

FIG. 4 Band inversion with spin-orbit coupling could lead to topological insulator or Dirac/Weyl semimetal.

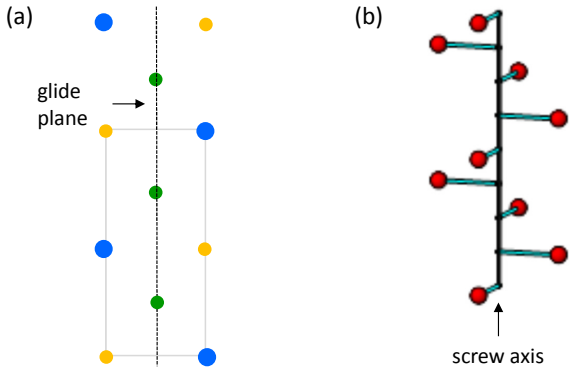

FIG. 5 Two examples of nonsymmorphic symmetry: (a) A glide plane consists of a mirror reflection (with respect to the mirror plane), and a translation the dotted line by 1/2 primitive lattice vector. (b) A screw axis consists of a π-rotation around the axis, and a translation along the axis by 1/2 primitive lattice vector.

So

$$\mathsf{H} \to \mathsf{H}' = \mp v(\mathbf{k} + \mathbf{k}_0) \cdot \boldsymbol{\sigma}. \tag{1.17}$$

Therefore, if there is SIS, then there must be another nodal point at $-\mathbf{k}_0$ with opposite helicity.

When both TR and SI symmetries exist, each node consists of two monopoles with opposite charges. The net topological charge of a nodal point (with 4 levels) is zero, and this Dirac node is not stable against perturbations (see Table I).

Note that when there is only SIS (but no TRS), then the minimum number of Weyl points in a solid is 2. If there is only TRS (but no SIS), then the minimum number is 4 (see Chap 7 of Meng, 2012), since TR-doublet would have a partner doublet with opposite helicity, as required by the Nielsen-Ninomiya theorem.

C. From Dirac to Weyl

A Weyl point is topologically stable, but there is no systematic way to find it. On the other hand, a Dirac point is not protected by topology, but there is some guideline for discovering it. Therefore, we can first search for Dirac semimetal, then break TRS or SIS to generate Weyl points.

There are several ways to engineer or search for the Dirac semimetal (Armitage *et al.*, 2018). First, one can change the composition of a hybrid structure, or change the material composition of a compound to produce a phase transition between a normal insulator and a topological insulator. At the critical point, the energy gap is closed and we could have the degenerate point. More details can be found in next Sec.

Second, we can rely on the mechanism of band inversion. Recall that in a TI, SOC would open a gap at the crossing point of inverted bands. However, if the two bands belong to different irreducible representations (IRs) of the space group of a crystal, then they would not couple with each other to open a gap (Fig. 4). This symmetry-protected degenerate point often occurs along a symmetry axis. Several Dirac materials belong to this class, such as alkali pnictides A_3B (A=Na, K, Rb ..., B=As, Sb, Bi ...), and Cd_3As_2.

Before introducing the third way of search, some knowledge of space group is required:

1) In a BZ, certain **k**-points can be invariant (mod reciprocal lattice vector **G**) under some symmetry operations of a space group. A subgroup $G_{\mathbf{k}}$ of the space group of a crystal that leaves **k** invariant is called a **little group**. This **k**-point cannot be inside the Brillouin zone (except the origin), but is located at some high symmetry point on a BZ surface.

2) Space groups can be divided into two classes: If, apart from lattice translation, all symmetry operations leave one point fixed, then the space group is **symmorphic**. If a fraction of primitive lattice translation is involved in symmetry operations, then the space group is **nonsymmorphic**. There are two new types of symmetry operations in nonsymmorphic space groups: **glide planes** or **screw axes** (Fig. 5). There are 157 nonsymmorphic space groups out of 230 space groups.

To find a Dirac semimetal, we can look for materials with a little group $G_{\mathbf{k}}$ that has four-dimensional IR (FDIR) at some high symmetry **k**-point. Such a possibility can be excluded for any symmorphic group in 3D. Therefore, one only need to search within crystals with nonsymmorphic symmetry. At that high-symmetry **k**-point, 4 levels would cross each other to form a Dirac point. These points can be located on the face, edge, or corner of a BZ surface.

The analysis based on 4-state Hamiltonians in previous Chap, with the addition of crystal symmetry (not discussed there), is relevant to the crossing of 4 levels near a Dirac point. There are several possible patterns

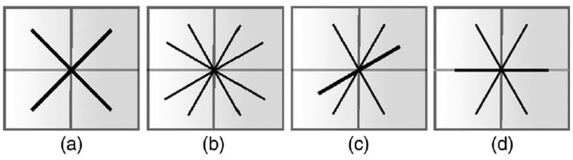

FIG. 6 Different patterns of level splitting near a Dirac point.

of the crossing, as shown in Fig. 6. For the band-inversion mechanism, the space inversion operator Π can be 1 or τ_z. However, if $\Pi = \tau_x$, then it is an exchange of orbital degree of freedom, which can be associated with the exchange of sublattices produced by a non-primitive translation in a nonsymmorphic space group (Armitage *et al.*, 2018).

After having the Dirac semimetal, one can break the TRS or the SIS to obtain the Weyl semimetal. The candidates for the former case includes, e.g., $GdPtBi$, and some magnetic Heusler compounds. For the latter case, we have WTe_2, $MoTe_2$, $RhSi$, and the $TaAs$ family (Zhang *et al.*, 2021).

D. The Burkov-Balent multilayer model

Without diving into the subject of space group symmetry, here we introduce a simplified model proposed by Burkov and Balent (Burkov and Balents, 2011) to produce a Dirac/Weyl point. Consider a structure with alternating layers of normal insulators (NI) and topological insulators (TI) stacked along the z-axis (see Fig. 7). Coupling of the top and down surface states (SS) of a TI layer is written as t_s; coupling of SS between nearest-neighbor TI layers is written as t_d.

When the intra-layer coupling is larger than the inter-layer coupling ($t_s > t_d$), the whole structure is similar to a NI. On the other hand, when $t_d > t_s$, the whole structure is similar to a TI. By tuning the relative strength between t_s and t_d, one can induce a topological phase transition at certain critical value. At that value the bulk gap is expected to close, probably producing a point degeneracy.

However, from the analysis in previous section, we know that with both TRS and SIS, this degenerate (Dirac) point would be unstable. The degeneracy would be lifted when one of the symmetry is broken.

For one TI slab doped with magnetic elements, the Hamiltonian with the SS coupling is,

$$\mathsf{H} = v\tau_z \otimes (\boldsymbol{\sigma} \times \mathbf{k}_\perp) \cdot \hat{z} + m1 \otimes \sigma_z + t_s\tau_x \otimes 1, \quad (1.18)$$

in which $\boldsymbol{\tau}$ accounts for the up and down layers degree of freedom, and m is the magnetization. From now on we will drop the $\otimes$ sign.

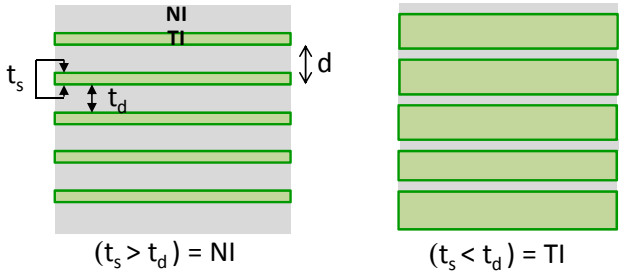

FIG. 7 A multi-layer structure with alternating layers of normal insulator (NI) and topological insulator (TI).

For multiple-layers, we have

$$\begin{aligned}\hat{\mathsf{H}} &= \sum_l \left[v\tau_z(\boldsymbol{\sigma} \times \mathbf{k}_\perp) \cdot \hat{z} + m\sigma_z + t_s\tau_x\right] c_l^\dagger c_l \\ &+ \sum_l t_d(\tau_+ c_l^\dagger c_{l+1} + \tau_- c_l^\dagger c_{l-1}), \end{aligned} \quad (1.19)$$

where $\tau_\pm = (\tau_x \pm i\tau_y)/2$, $c_l = (c_{lu}, c_{ld})^T$ is a 2-component operator such that $\tau_+ c_l^\dagger c_{l+1} = c_{lu}^\dagger c_{l+1d} \cdots$ etc.

Assume there are N (NI+TI)-layers with period d, and impose the periodic BC along z-axis. Using the Fourier transformation,

$$c_l^\dagger = \frac{1}{\sqrt{N}} \sum_{k_z} e^{ildk_z} c_{k_z}^\dagger. \quad (1.20)$$

one has,

$$\begin{aligned}\hat{\mathsf{H}} &= \sum_{k_z} \Big[v\tau_z(\boldsymbol{\sigma} \times \mathbf{k}_\perp) \cdot \hat{z} c_{k_z}^\dagger c_{k_z} \\ &+ m\sigma_z c_{k_z}^\dagger c_{k_z} \\ &+ t_s\tau_x c_{k_z}^\dagger c_{k_z} \\ &+ t_d(e^{-ik_z d}\tau_+ c_{k_z}^\dagger c_{k_z} + e^{ik_z d}\tau_- c_{k_z}^\dagger c_{k_z})\Big] \quad (1.21) \\ &= \sum_{k_z} \begin{pmatrix} \mathsf{h}_0 + m\sigma_z & t_s + t_d e^{-ik_z d} \\ t_s + t_d e^{ik_z d} & -\mathsf{h}_0 + m\sigma_z \end{pmatrix} c_{k_z}^\dagger c_{k_z}, \\ &\equiv \sum_{k_z} \mathsf{H}_{k_z} c_{k_z}^\dagger c_{k_z}, \quad (1.22) \end{aligned}$$

where $\mathsf{h}_0 = v(\boldsymbol{\sigma} \times \mathbf{k}_\perp) \cdot \hat{z}$, and

$$\begin{aligned}\mathsf{H}_{k_z} &= \tau_z \mathsf{h}_0 + m\sigma_z \\ &+ t_s\tau_x + t_d(e^{-ik_z d}\tau_+ + e^{ik_z d}\tau_-). \end{aligned} \quad (1.23)$$

Each k_z-subsystem is independent of each other.

Under the unitary transformation (Burkov *et al.*, 2011),

$$\mathsf{U} = \begin{pmatrix} 1 & 0 \\ 0 & \sigma_z \end{pmatrix} \quad (1.24)$$

one has

$$\tau_{x,y} \to \mathsf{U}^\dagger \tau_{x,y} \mathsf{U} = \tau_{x,y}\sigma_z, \quad (1.25)$$
$$\sigma_{x,y} \to \mathsf{U}^\dagger \sigma_{x,y} \mathsf{U} = \tau_z \sigma_{x,y}. \quad (1.26)$$

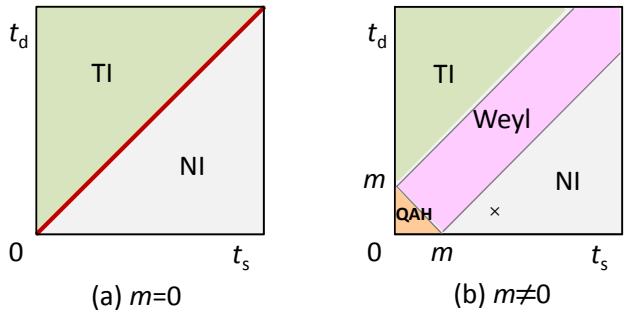

FIG. 8 (a) With both TRS and SIS, the critical line at $t_s = t_d$ are composed of unstable Dirac points. (b) After breaking the TRS with magnetization m, a Dirac point in (a) separates to two Weyl points and there is a finite region of Weyl semimetal phase. The gapped phase on the lower left is a semi-quantum anomalous Hall phase. As m gets larger, the point marked with× is first engulfed by the Weyl phase, then by the semi-QAH phase.

τ_z and σ_z are not changed. After the transformation,

$$\begin{aligned} \mathsf{H}_{k_z} &= \mathsf{h}_0 + m\sigma_z \\ &+ [t_s\tau_x + t_d(e^{-ik_z d}\tau_+ + e^{ik_z d}\tau_-)]\sigma_z. \end{aligned} \quad (1.27)$$

One can rotate the $\boldsymbol{\tau}$ on the 2nd line without changing the first line. Thus, the Hamiltonian is decomposed to 2 diagonal blocks,

$$\begin{aligned} \mathsf{H}_{k_z} &= \mathsf{h}_0 + \underbrace{\left[m + \tau_z\sqrt{t_s^2 + t_d^2 + 2t_s t_d\cos(k_z d)}\right]}_{M_{\tau_z}(k_z)}\sigma_z \\ &= v(\boldsymbol{\sigma}\times\mathbf{k}_\perp)\cdot\hat{z} + M_{\tau_z}(k_z)\sigma_z, \end{aligned} \quad (1.28)$$

where $M_\pm(k_z)$ can be considered as the effective magnetization of the 2D electron gas in the k_z-layer.

Finally, the 2×2-blocks can be easily diagonalized to get the eigenvalues,

$$\varepsilon_\pm^{\tau_z} = \pm\sqrt{v^2(k_x^2+k_y^2) + M_{\tau_z}^2(k_z)}. \quad (1.29)$$

Let $m > 0$, then $M_+(k_z)$ is always positive, and $\varepsilon_\pm^+$ has a finite gap. On the other hand, $\varepsilon_\pm^-$ can be gapless if $M_-(k_z) = 0$, or

$$\cos(k_0 d) = \frac{m^2 - (t_s^2 + t_d^2)}{2t_s t_d}. \quad (1.30)$$

That is, if

$$\underbrace{|t_s - t_d|}_{m_{c1}} \le m \le \underbrace{|t_s + t_d|}_{m_{c2}}, \quad (1.31)$$

then there are a pair of Weyl nodes at $\pm k_0\hat{z}$ (see Fig. 9).

If $m < |t_s - t_d|$, then Eq. (1.30) has no real solution, and $M_-(k_z) < 0$. If $m > |t_s - t_d|$, then Eq. (1.30) has no real solution, and $M_-(k_z) > 0$. For small m, the material is a trivial insulator. The pair of Weyl nodes appear at

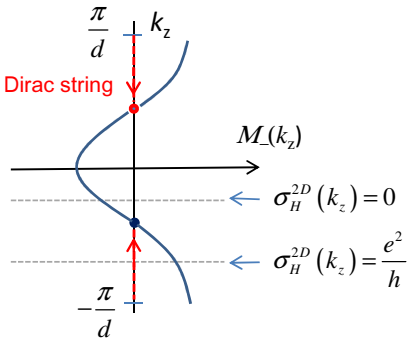

FIG. 9 $M_-(k_z)$ plotted as a function of k_z. The plot is rotated by 90 degrees.

$k_z d = \pi$ when $m = m_{c1}$. They move apart along the k_z-axis when $m > m_{c1}$, and merge with each other again at $k_z = 0$ when $m = m_{c2}$ (see Fig. 10). After that, the energy gap is re-opened, but the system becomes a non-trivial insulator (see Fig. 8(b)).

We now focus on the Weyl semimetal phase. As shown in Eq. (1.22), the system is composed of decoupled 2D sub-systems, each has their own k_z-layer of 2D BZ . Since the Weyl point is a 3D monopole, it has a string of gauge singularity (Dirac string). The location of the string is gauge dependent, but they should connect the two Weyl nodes (see Fig. 10). The 2D k_z-layers within $|k_z| < k_0$ ($M_-(k_z) < 0$) do not intersect with the gauge singularity, and the first Chern number $C_1 = 0$. On the other hand, the k_z-layers outside of that range would intersect with the Dirac string. At the point of intersection is a vortex singularity of the gauge potential. This leads to $C_1 = 1$, and $\sigma_H^{2D}(k_z) = e^2/h$ for each of the 2D-subsystem. See Sec **??** for the discussion of the vortex in the BZ of a quantum Hall system.

As a result, the 3D Hall conductivity is

$$\begin{aligned} \sigma_H^{3D} &= \frac{1}{L_z}\sum_{k_z}\sigma_H^{2D}(k_z) \\ &= \int_{-\pi/d}^{\pi/d}\frac{dk_z}{2\pi}\sigma_H^{2D}(k_z) = \frac{e^2}{h}\frac{\bar{k}_0}{\pi}, \end{aligned} \quad (1.32)$$

where $\bar{k}_0 = \pi/d - k_0$ is half the length of the Dirac string.

When $m = m_{c2}$, the two nodes merge at $k_z = 0$, and the Dirac string spans the whole k_z-axis. After that, the system enters the semi-quantum anomalous Hall phase with

$$\sigma_H^{3D} = \frac{e^2}{h}\frac{1}{d}. \quad (1.33)$$

In a magnetic Weyl semimetal that breaks time-reversal symmetry, it is possible to have such an anomalous Hall state (Liu *et al.*, 2018).

Some of the Weyl semimetals proposed early are antiferromagnetic (that break TRS), such as the pyrochlore irridates $A_2Ir_2O_7(A = Y, Eu, Nd...)$. Other Weyl semimetal with antiferromagnetic order are

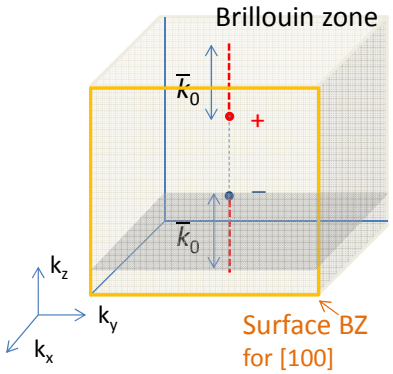

FIG. 10 A pair of Weyl points appear at $k_z = \pi$ when $m = m_{c1}$. They stretch out a Dirac string (red dotted lines) at larger m, and finally merge with each other at $m = m_{c2}$, but leaving a full Dirac string behind.

Mn_3Sn, Mn_3Gn. Later it was found that some Heusler compounds are good candidates of magnetic Weyl semimetals. For example, the $LnPtBi$ family ($Ln = Gd, Nd$ ...) of half-Heusler compound. Weyl nodes are also predicted to be common in cobalt-based magnetic Heusler compound, such as $Co_2YZ(Y = V, Zr, Nb...; Z = Si, Ge.Ne...)$, and Co_2MnAl, which have their Weyl points near Fermi energies. See Armitage *et al.*, 2018, Narang *et al.*, 2020 for more details. Furthermore, in the so-called **Kramer-Weyl semimetal**, the Weyl points are located at TRIMs. Therefore, the Fermi arcs span across the BZ (Chang *et al.*, 2018), and one could have the QAH state.

1. Fermi arc of surface states

Divide the space into two parts, with the magnetization

$$\begin{aligned} m(x) &< |t_s - t_d| \text{ for } x < 0, \text{ or } M_-(k_z) < 0 \text{ (NI)} \\ m(x) &> |t_s - t_d| \text{ for } x > 0, \text{ or } M_-(k_z) > 0 \text{ (WSM)} \end{aligned}$$

and $m(x)$ increases monotonically from one side to the other. Ignoring the $M_+(k_z)$ block. The remaining two-state Hamiltonian for a 2D sub-system is (see Eq. (1.28))

$$\mathsf{H}_{k_z} = \mathsf{h}_0 + \underbrace{\left[m(x) - \sqrt{t_s^2 + t_d^2 + 2t_s t_d \cos(k_z d)}\right]}_{M_-^{k_z}(x)} \sigma_z. \tag{1.34}$$

Similar to the analysis of the edge states of the QWZ model in Chap. **??**, first replace k_x by the differential operator $\frac{1}{i}\frac{\partial}{\partial x}$. One then solves the following differential equation to find the edge state,

$$\begin{pmatrix} M_-^{k_z}(x) & v\left(\frac{\partial}{\partial x} + k_y\right) \\ v\left(-\frac{\partial}{\partial x} + k_y\right) & -M_-^{k_z}(x) \end{pmatrix} \phi_s^{k_z} = \varepsilon_s^{k_z}(k_y)\phi_s^{k_z}. \tag{1.35}$$

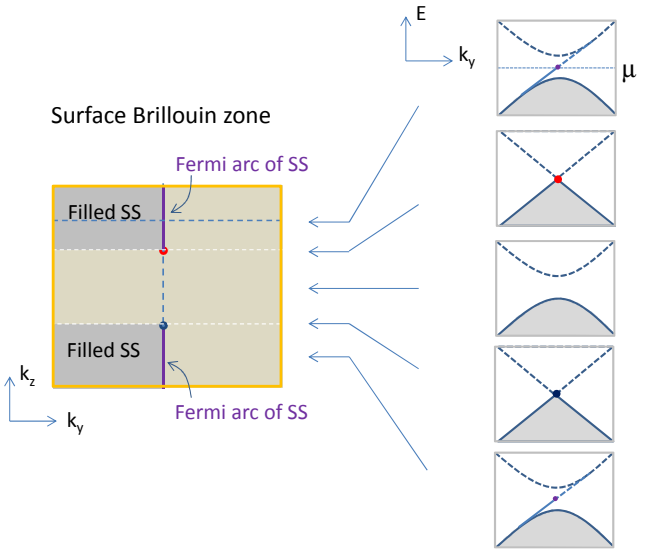

FIG. 11 Fermi arc of the SS in a 2D surface BZ. Five slices of the 1D edge BZ of the 2D k_z-subsystem are shown on the right.

A trial solution that is localized near $x = 0$ is,

$$\phi_s^{k_z}(x) = e^{-\frac{1}{v}\int_0^x dx' M_-^{k_z}(x)} \begin{pmatrix} 1 \\ 1 \end{pmatrix}. \tag{1.36}$$

One can verify that it is indeed an eigenstate, with eigenvalue $\varepsilon_s^{k_z}(k_y) = vk_y$, which is linear in k_y and independent of k_z.

The energy dispersion of the surface states is a 2D surface in the 3D BZ. The surface BZ for the [100] surface is shown in Fig. 11, with 5 slices of the energy dispersion shown on the right. A 2D subsystem with $C_1 = 0$ is a trivial 2D insulator, which has no edge state. A 2D subsystem with $C_1 = 1$ is similar to a 2D quantum Hall system, which has chiral edge state. The electrons fill up to a Fermi point in its 1D edge BZ. By connecting these points from different k_z's, one sees that the SS electrons of the Weyl semimetal would fill up to a Fermi line (aka **Fermi arc**, Wan *et al.*, 2011). For more details, see Yang *et al.*, 2011 and Okugawa and Murakami, 2014. Also see Potter *et al.*, 2014 for an illuminating analysis of the SS and the Fermi arc.

Experimentally, transition metal monopnictides such as $TaAs$ (Lv *et al.*, 2015; Xu *et al.*, 2015b), and $NbAs$ (Xu *et al.*, 2015a) are among the first to be confirmed as Weyl semimetals, and their Fermi arcs observed.

2. Property of Fermi arc

Using a two-band model with *a pair* of Weyl nodes, one can explore some properties of the Fermi arc in details (Okugawa and Murakami, 2014). In Fig. 12(a), we see the energy dispersion near the Weyl points of the bulk states. If the Weyl semimetal has boundaries, then there

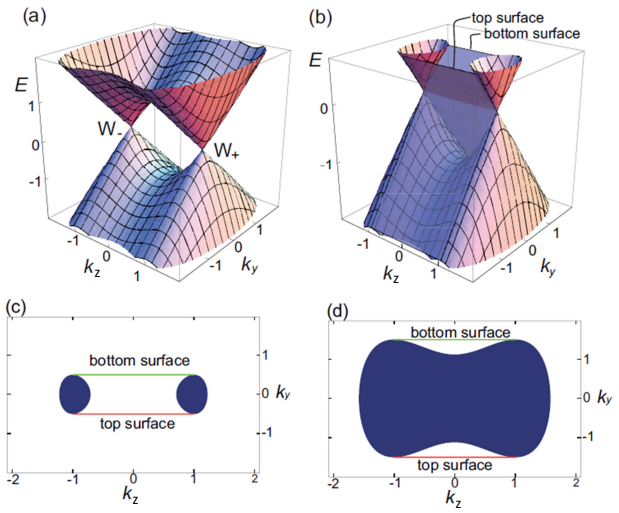

FIG. 12 (a) Weyl points from the bulk energy bands. (b) Energy dispersions of the bulk states and the surface states. (c) Two Fermi seas are connection by Fermi arcs. (d) At higher chemical potential, two Fermi seas merge as one. Fig from Okugawa and Murakami, 2014.

are 2D energy sheets of surface states stretching between two Weyl nodes (Fig. 12(b)). The SSs from the top and the bottom boundaries have opposite slopes along the k_y direction. When the chemical potential μ is at the energy of the Weyl-point, it would cut through the 2D energy sheet of the SS, forming a Fermi arc between two Weyl points. This is consistent with the analysis in previous Section.

If μ is away from, e.g., higher than, the energy of the Weyl points, then there are puddles of Fermi sea around the Weyl points. These puddles are connected by Fermi arcs (Fig. 12(c)). Furthermore, the Fermi arc would be tangent to the edge of the Fermi sea (Haldane, 2014).

When μ gets higher, the two puddles would eventually merge with each other (Fig. 12(d)). Such a change of the topology of the Fermi surface is sometimes referred to as a **Lifshitz transition**.

E. Beyond linear Weyl point

A Weyl point with linear dispersion is the simplest form of the point degeneracy. Other types of degeneracy could also be related to topology and have some interesting physical effect. Here I list some of the generalizations beyond this simplest case:

1. Near a degenerate point, the energy dispersion can be quadratic, cubic, or of higher orders. This would generate higher topological charges, and multiple Fermi arcs between Weyl points.
2. The Dirac cone can be slightly slanted, or highly slanted to the degree that one Fermi level can cut through both cones. This is called **type-II Weyl fermion**.
3. Near a degenerate point, there could be a crossing between 3 levels (spin-1 Weyl fermion), 4 levels with nonzero topological charge (spin 3/2 Weyl fermion), or more.
4. Beyond point degeneracy, one could have nodal line, nodal loop, nodal chain (connected loops), linked nodal loops (no contact between loops), or nodal plane. In general, an electron circling a nodal line would acquire a Berry phase π.

Obviously, mixed types of degeneracy are also possible. For example, a three-level crossing with quadratic dispersion. There are numerous works exploring these possibilities. One may see Lv *et al.*, 2021 and the references therein for some more details.

Exercise

1. Instead of breaking TRS, one can break the SIS of the Burkov-Balent model, for example, by unbalancing the top-bottom layers of the TI slabs. That is, by adding a term $V_0\tau_z$ to the Hamiltonian ($t_{s,d} > 0$),

$$\begin{aligned} \mathsf{H} &= \tau_z \mathsf{h}_0 + V_0\tau_z \\ &+ t_s\tau_x + t_d(e^{-ik_z d}\tau_+ + e^{ik_z d}\tau_-), \end{aligned} \tag{1.37}$$

where $h_0 = v(\boldsymbol{\sigma} \times \mathbf{k}_\perp) \cdot \hat{z}$.
(a) Given the SI operator $\Pi = \tau_x$, show that the Hamiltonian with $V_0 = 0$ has SIS, $\Pi\mathsf{H}(\mathbf{k})\Pi^{-1} = \mathsf{H}(-\mathbf{k})$, while V_0 breaks it.
(b) Switch from the basis $\boldsymbol{\tau} \otimes \boldsymbol{\sigma}$ to the basis $\boldsymbol{\sigma} \otimes \boldsymbol{\tau}$, perform a rotation in $\boldsymbol{\tau}$-space to block-diagonalize the Hamiltonian, then find out the eigenvalues $\varepsilon_\pm^{\sigma_z}$ of H.
2. Following Prob. 1, (a) show that when $t_s = t_d$, the middle two bands touch at a circle of line degeneracy at $k_z = \pi/d$. Such a degeneracy requires the fine-tuning of t_s and t_d, and therefore is not robust.
(b) Break the rotational symmetry around k_z by having

$$t_{s,d} = t^0_{s,d} + t'_{s,d}k_x^2 \tag{1.38}$$

$$= t^0_{s,d} + t'_{s,d}k_\perp^2 \cos^2\theta. \tag{1.39}$$

Show that, when $t_s = t_d$, there are point degeneracies at

$$\cos 2\theta = \frac{2(t_s^0 - t_d^0)}{k_\perp^2(t'_d - t'_s)} - 1. \tag{1.40}$$

(c) The multilayer structure is a normal insulator when $t_s^0 > t_d^0$. Assume $t'_s > t'_d$, decrease the value of t_s^0 and investigate the creation and annihilation of Weyl points. (Ref: Halász and Balents, 2012)

References

Armitage, N. P., E. J. Mele, and A. Vishwanath, 2018, Rev. Mod. Phys. **90**, 015001.
Burkov, A. A., and L. Balents, 2011, Phys. Rev. Lett. **107**, 127205.
Burkov, A. A., M. D. Hook, and L. Balents, 2011, Phys. Rev. B **84**, 235126.

Chang, G., B. J. Wieder, F. Schindler, D. S. Sanchez, I. Belopolski, S.-M. Huang, B. Singh, D. Wu, T.-R. Chang, T. Neupert, S.-Y. Xu, H. Lin, *et al.*, 2018, Nature Materials **17**(11), 978.

Chang, M.-C., and M.-F. Yang, 2015, Phys. Rev. B **92**, 205201.

Felsager, B., 1998, *Geometry, particles and fields* (Springer-Verlag, New York).

Halász, G. B., and L. Balents, 2012, Phys. Rev. B **85**, 035103.

Haldane, F. D. M., 2014, Attachment of surface "fermi arcs" to the bulk fermi surface: "fermi-level plumbing" in topological metals, eprint 1401.0529.

Liu, E., Y. Sun, N. Kumar, L. Muechler, A. Sun, L. Jiao, S.-Y. Yang, D. Liu, A. Liang, Q. Xu, J. Kroder, V. Süß, *et al.*, 2018, Nature Physics **14**(11), 1125.

Lv, B. Q., T. Qian, and H. Ding, 2021, Rev. Mod. Phys. **93**, 025002.

Lv, B. Q., H. M. Weng, B. B. Fu, X. P. Wang, H. Miao, J. Ma, P. Richard, X. C. Huang, L. X. Zhao, G. F. Chen, Z. Fang, X. Dai, *et al.*, 2015, Phys. Rev. X **5**, 031013.

Meng, T., 2012, *Quantum critical matter: Quantum phase transitions with multiple dynamics and Weyl superconductors*, Ph.D. thesis, •University of Köln.

Milnor, J. W., 1965, *Topology from the differential viewpoint* (The University Press of Virginia, Charlottesiville).

Narang, P., C. A. C. Garcia, and C. Felser, 2020, Nature Materials .

Nielsen, H. B., and M. Ninomiya, 1981a, Nuclear Physics B **185**(1), 20.

Nielsen, H. B., and M. Ninomiya, 1981b, Nuclear Physics B **193**(1), 173.

Okugawa, R., and S. Murakami, 2014, Phys. Rev. B **89**, 235315.

Potter, A. C., I. Kimchi, and A. Vishwanath, 2014, Nature Communications **5**, 5161.

Wan, X., A. M. Turner, A. Vishwanath, and S. Y. Savrasov, 2011, Phys. Rev. B **83**, 205101.

Xu, S.-Y., N. Alidoust, I. Belopolski, Z. Yuan, G. Bian, T.-R. Chang, H. Zheng, V. N. Strocov, D. S. Sanchez, G. Chang, C. Zhang, D. Mou, *et al.*, 2015a, Nat Phys **11**(9), 748.

Xu, S.-Y., I. Belopolski, N. Alidoust, M. Neupane, G. Bian, C. Zhang, R. Sankar, G. Chang, Z. Yuan, C.-C. Lee, S.-M. Huang, H. Zheng, *et al.*, 2015b, Science **349**(6248), 613.

Yang, K.-Y., Y.-M. Lu, and Y. Ran, 2011, Phys. Rev. B **84**, 075129.

Zhang, C., Y. Zhang, H.-Z. Lu, X. C. Xie, and F. Xiu, 2021, Nature Reviews Physics **3**(9), 660.